Available online at www.eccomasproceedia.org
Eccomas Proceedia UNCECOMP (2025) 72-83

ECCOMAS
Proceedia

UNCECOMP 2025
6th ECCOMAS Thematic Conference on
Uncertainty Quantification in Computational Science and Engineering
M. Papadrakakis, V. Papadopoulos, G. Stefanou (eds.)
Rhodes Island, Greece, 15-18 June 2025

EFFICIENT CONFIDENCE BOUND ESTIMATION FOR A DYNAMIC COMPOSITE PLATE WITH EPISTEMIC UNCERTAINTIES USING NON-INTRUSIVE IMPRECISE STOCHASTIC SIMULATION

Everton Grotti[1], Matteo Broggi[2], Herbert M. Gomes[1], and Michael Beer[2]

[1]Federal University of Rio Grande do Sul
Department of Mechanical Engineering, Av. Sarmento Leite, 425, Porto Alegre, RS, Brazil
e-mail: ewerton.grotti@ufrgs.br, herbert@mecanica.ufrgs.br

[2]Leibniz University Hannover
Institute for Risk and Reliability, Callinstr. 34, 30167, Hannover, Germany
broggi@irz.uni-hannover.de, beer@irz.uni-hannover.de

Abstract

This study investigates the dynamic response of composite plates under epistemic uncertainties, focusing on confidence bounds for vertical displacements. A composite plate with a clamped-free-free-free boundary condition is modeled using the Finite Element Method (FEM) based on Mindlin plate theory. The material properties and loadings are characterized using probabilistic distributions and contain epistemic uncertainty. To approximate the confidence bounds (envelopes) for output variables, Non-Intrusive Imprecise Stochastic Simulation (NISS) method is applied, and the resulting High-Dimensional Model Representation (HDMR) equations are optimized to obtain the confidence limits for CDFs. This procedure provides a computationally efficient approach compared to the resource-intensive nested double-loop Monte Carlo Simulation (MCS) for epistemic variables. The results provide a comparative analysis of confidence bounds generated by both methods, highlighting the efficiency and the associated error of the proposed NISS based framework.

Keywords: Epistemic Uncertainty, Non-Intrusive Imprecise Stochastic Simulation, Double-Loop Monte Carlo, Composite Plate, Vibration.

ISSN:2623-3339
Peer-review under responsibility of the organizing committee of UNCECOMP 2025.
doi: 10.7712/120225.12341.21417

1 INTRODUCTION

In the fields of engineering and material sciences, understanding the behavior of composite materials under uncertain conditions is a growing concern. Composite materials are known for their lightweight combined with high-strength properties and are widely used in applications such as aerospace, automotive, and civil engineering. However, their performance is influenced by a multitude of factors, ranging from material properties to excitation forces, many of which are inherently uncertain [1, 2]. These uncertainties stem from complex manufacturing processes, variations in constituent material properties, inherent defects, and diverse excitation loads and boundary conditions.

Probabilistic descriptions of uncertainties in composite materials are often hindered by insufficient data [3]. As a result, epistemic uncertainty presents a significant challenge, potentially compromising the safety and efficiency of critical designs. Direct approaches to propagating epistemic uncertainty, such as the nested double-loop Monte Carlo Simulation (MCS) method, require an exceptionally large number of deterministic simulations, which often lead to computationally intractable procedures [4]. This issue is made worse in engineering applications where the deterministic simulations are computationally demanding, such as those based on the finite element method (FEM). To reduce computational costs, metamodels are frequently employed, such as Kriging, Radial Basis Function, Polynomial Chaos Expansion, and Neural Networks, as detailed in [1].

Approaches for problems involving epistemic uncertainties include the interval method [5-8], fuzzy theory [9-13], among others. These are called non-probabilistic methods and have been popularly adopted in structural dynamics [14]. The approach named imprecise probabilistic method, also called P-box, has also gained attention [15, 16], where a distribution with uncertain statistics is assumed. Among the recent advancements in this category, the Non-Intrusive Imprecise Stochastic Simulation (NISS) has emerged as a promising technique, as demonstrated in [17-20]. According to [21], the P-box model is still rarely applied to analyze the uncertainty of composites. This study aims at this gap by proposing a novel framework to efficiently tackle dynamic problems involving epistemic uncertainties. This work represents the first attempt in the literature to apply NISS to composite vibration problems solved in the time domain to the best of the author's knowledge.

This study is organized into five sections, beginning with this introduction as the first section. The second section provides an overview of the theoretical framework related to the simulation of the composite plate used in this work. The third section introduces the methods for addressing epistemic uncertainty, specifically NISS and MCS. An illustrative example with the corresponding solution is described in the fourth section. Finally, the study concludes with a summary of findings and insights in the fifth section.

2 COMPOSITE PLATES THEORY

Composite materials are engineered by combining two or more constituent substances with significantly different mechanical properties. This combination results in a material with characteristics distinct from those of its individual components. While composites exhibit exceptional mechanical properties, their complex heterogeneous structures and anisotropic nature pose unique challenges for traditional analytical methods. The FEM overcomes these challenges by discretizing the material into smaller, manageable elements [22], allowing for detailed simulations of stress distribution, deformation and failure mechanisms.

2.1 Finite Element Method for Mindlin Plates

The composite plate in this study is simulated using FEM by means of Mindlin plate theory (first-order shear deformation theory, FSDT). According to [23], the displacement field, in this case, is

$$u(x,y,z) = u_0(x,y) + z\theta_x(x,y), \tag{1}$$

$$v(x,y,z) = v_0(x,y) + z\theta_y(x,y), \tag{2}$$

$$w(x,y,z) = w_0(x,y), \tag{3}$$

where u, v, and w are the displacements in x, y, and z, respectively, θ_x is the rotation on the x axis, and θ_y is the rotation on the y axis.

$$\begin{Bmatrix} \varepsilon_{xx} \\ \varepsilon_{yy} \\ \gamma_{xy} \\ \gamma_{xz} \\ \gamma_{yz} \end{Bmatrix} = \left\{ \frac{\partial u}{\partial x} \quad \frac{\partial v}{\partial y} \quad \left(\frac{\partial u}{\partial y} + \frac{\partial v}{\partial x}\right) \quad \left(\frac{\partial u}{\partial z} + \frac{\partial w}{\partial x}\right) \quad \left(\frac{\partial v}{\partial z} + \frac{\partial w}{\partial y}\right) \right\}^T \tag{4}$$

To define the stiffness matrix, one should start from the strain energy and integrate it throughout each layer over the thickness direction. The membrane part of the stiffness matrix $\boldsymbol{K}_{mb}^{(e)}$, the membrane-bending coupling components $\boldsymbol{K}_{mb}^{(e)}$ and $\boldsymbol{K}_{bm}^{(e)}$, the bending $\boldsymbol{K}_{bb}^{(e)}$ and the shear component $\boldsymbol{K}_{ss}^{(e)}$ are obtained as follows

$$\boldsymbol{K}_{mm}^{(e)} = \sum_{k=1}^{nc} \int_A \boldsymbol{B}_m^T \boldsymbol{D_k} \boldsymbol{B_m} \, (z_{k+1} - z_k) dA \tag{5}$$

$$\boldsymbol{K}_{mb}^{(e)} = \sum_{k=1}^{nc} \int_A \boldsymbol{B}_m^T \boldsymbol{D_k} \boldsymbol{B_b} \frac{1}{2} \, (z_{k+1}^2 - z_k^2) dA \tag{6}$$

$$\boldsymbol{K}_{bm}^{(e)} = \sum_{k=1}^{nc} \int_A \boldsymbol{B_b^T} \boldsymbol{D_k} \boldsymbol{B_m} \frac{1}{2} \, (z_{k+1}^2 - z_k^2) dA \tag{7}$$

$$\boldsymbol{K}_{bb}^{(e)} = \sum_{k=1}^{nc} \int_A \boldsymbol{B_b^T} \boldsymbol{D_k} \boldsymbol{B_b} \frac{1}{3} \, (z_{k+1}^3 - z_k^3) dA \tag{8}$$

$$\boldsymbol{K}_{ss}^{(e)} = \sum_{k=1}^{nc} \int_A \boldsymbol{B_s^T} \boldsymbol{D_k} \boldsymbol{B_s} \, (z_{k+1} - z_k) dA \tag{9}$$

where nc is the number of layers, $\boldsymbol{D}$ is the rotated constitutive matrix, z_k is the coordinate for the k^{th} layer in the thickness direction with the reference being the middle plane of the composite plate as shown in Figure 1 (starting at $k = 1$ from the bottom). $\boldsymbol{B_m}$, $\boldsymbol{B_b}$ and $\boldsymbol{B_s}$ are the strain-displacement matrices for membrane, bending and shear, respectively, which hold information regarding the shape function. For this study, the shape function is assumed as a bilinear four-noded Q4 element as shown in [23].

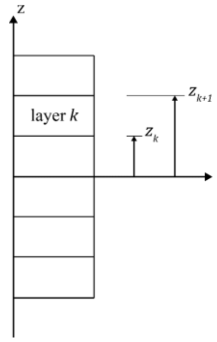

Figure 1: Laminated plate layer diagram. Based on Ferreira, 2014 [23].

Thus, the element stiffness matrix results in

$$\boldsymbol{K}^{(e)} = \boldsymbol{K}_{mm}^{(e)} + \boldsymbol{K}_{mb}^{(e)} + \boldsymbol{K}_{bm}^{(e)} + \boldsymbol{K}_{bb}^{(e)} + \boldsymbol{K}_{ss}^{(e)}. \tag{10}$$

The global stiffness matrix $\boldsymbol{K}$ is then assembled through superposition. The corresponding global mass matrix $\boldsymbol{M}$ is obtained in an analogous way.

2.2 Micromechanics for Elastic Properties

Using the constituents' properties it is possible to derive the mechanical properties of the composite plate. The elastic properties can be estimated by means of the Rule of Mixtures [24], defined as a function of the volume fraction of fibers and matrix.

$$E_1 = E_f V_f + E_m V_m \tag{11}$$

$$1/E_2 = V_f/E_f + V_m/E_m \tag{12}$$

$$V_m = 1 - V_f \tag{13}$$

where E_1 and E_2 are the longitudinal and transversal elastic modulus, V_f and V_m are the volume fraction of fiber and matrix, and E_f and E_m are the elastic modulus of fiber and matrix, respectively.

$$\nu_{12} = \nu_f V_f + \nu_m V_m \tag{14}$$

$$\nu_{21} = \nu_{12} E_2/E_1 \tag{15}$$

$$1/G_{12} = V_f/G_f + V_m/G_m \tag{16}$$

with ν_{21} and ν_{12} being the major and minor Poisson's ratio. G_f and G_m are the shear modulus of the fiber and matrix, and G_{12} is the in-plane shear modulus.

3 SIMULATION METHODS FOR DEALING WITH EPISTEMIC UNCERTAINTY

Epistemic uncertainty arises from a lack of knowledge or incomplete information in modeling complex systems. This chapter focuses on NISS and MCS approaches, providing a foundation for their application in subsequent sections of this study.

3.1 Nested Double-Loop Monte Carlo Simulation

A nested double-loop Monte Carlo simulation is the brute force approach when dealing with epistemic uncertainties. The following pseudocode in Table 1 portrays the code implemented in Matlab, used to generate the results in this study.

Define the number of samples for the inner loop, $\boldsymbol{N_{in}}$, and outer loop, $\boldsymbol{N_{out}}$.
Outer loop: for $\boldsymbol{i = 1}$ to $\boldsymbol{N_{out}}$
Sample the epistemic interval of each epistemic parameter.
Inner loop: for $\boldsymbol{j = 1}$ to $\boldsymbol{N_{in}}$
Sample the uncertain variables using the epistemic parameters $\boldsymbol{i}$.
end
Apply the $\boldsymbol{N_{in}}$ sampled uncertain variables in the desired function.
end
Generate one CDF for each set of $\boldsymbol{N_{in}}$ samples of the desired function.
Find the minimum and the maximum from all CDFs in each PQ (probability quantile).
Output: Build the graphical representation of the p-box using the set of minima and maxima extracted from the CDFs in each PQ.

Table 1: Pseudocode for double-loop Monte Carlo.

3.2 Non-intrusive Imprecise Stochastic Simulation

To deal with epistemic uncertainty while avoiding the high cost of the double-loop MCS, the NISS framework may be used. This method was proposed by Wei et al. [17] and uses a combination of mathematical techniques like HDMR decomposition (High Dimensional Model Representation), and importance sampling to approximate quantities of interest such as mean, standard deviation, and failure probability. In Wei et al. [17], local (cut-HDMR) and global (RS-HDMR) approaches are presented, where the local approach is more precise around the chosen combination of epistemic parameters, called $\boldsymbol{\theta}^*$ (i.e. the mean point of the interval).

For either cut-HDMR or RS-HDMR, the final equation for the quantity of interest should be built as

$$E_y(\boldsymbol{\theta}) = E_{y0} + \sum_{i=1}^{d} E_{yi}(\theta_i) + \sum_{1 \le i < j \le d} E_{yij}(\boldsymbol{\theta}_{ij}) + \cdots + E_{y12..d}(\boldsymbol{\theta}), \tag{17}$$

which, for cut-HDMR, follows

$$\begin{cases} \hat{E}_{cut\ y0}(\boldsymbol{\theta}^*) = \dfrac{1}{N}\displaystyle\sum_{k=1}^{N} y^{(k)} \\ \hat{E}_{cut\ yi}(\theta_i) = \dfrac{1}{N}\displaystyle\sum_{k=1}^{N} y^{(k)}\, r_{cut\ i}\left(\boldsymbol{x}^{(k)} \middle| \theta_i, \boldsymbol{\theta}^*\right) \\ \hat{E}_{cut\ yij}(\theta_{ij}) = \dfrac{1}{N}\displaystyle\sum_{k=1}^{N} y^{(k)}\, r_{cut\ ij}\left(\boldsymbol{x}^{(k)} \middle| \theta_{ij}, \boldsymbol{\theta}^*\right) \end{cases}, \tag{18}$$

$$\begin{cases} r_{cut\,i}\left(\boldsymbol{x}^{(k)}\middle|\theta_i,\boldsymbol{\theta}^*\right) = \dfrac{f_X\left(\boldsymbol{x}^{(k)}\middle|\theta_i,\boldsymbol{\theta}^*_{-i}\right)}{f_X\left(\boldsymbol{x}^{(k)}\middle|\boldsymbol{\theta}^*\right)} - 1 \\ r_{cut\,ij}\left(\boldsymbol{x}^{(k)}\middle|\theta_{ij},\boldsymbol{\theta}^*\right) = \dfrac{f_X\left(\boldsymbol{x}^{(k)}\middle|\boldsymbol{\theta}_{ij},\boldsymbol{\theta}^*_{-ij}\right)}{f_X\left(\boldsymbol{x}^{(k)}\middle|\boldsymbol{\theta}^*\right)} - \dfrac{f_X\left(\boldsymbol{x}^{(k)}\middle|\theta_i,\boldsymbol{\theta}^*_{-i}\right)}{f_X\left(\boldsymbol{x}^{(k)}\middle|\boldsymbol{\theta}^*\right)} - \dfrac{f_X\left(\boldsymbol{x}^{(k)}\middle|\theta_j,\boldsymbol{\theta}^*_{-j}\right)}{f_X\left(\boldsymbol{x}^{(k)}\middle|\boldsymbol{\theta}^*\right)} + 1 \end{cases}, \quad (19)$$

here, the indexes i and j may assume values between 1 and the total number of epistemic parameters. $\theta_i^{(k)}$ denotes the k-th sample point of θ_i, drawn from the joint samples. Similarly, $\boldsymbol{\theta}_{ij}^{(k)}$ represents the k-th sample point of $\boldsymbol{\theta}_{ij}$, also drawn from the joint samples. The term $\boldsymbol{\theta}_{ij}$ refers to the 2-dimensional vector composed of θ_i and θ_j, $\boldsymbol{\theta}$ is the vector of epistemic parameters, while $\boldsymbol{\theta}_{-i}$ denotes this same vector containing the epistemic parameters except for θ_i. $\hat{E}$ is the approximation for the quantity of interest, which in this case is the mean.

Other quantities of interests such as probability of failure and variance may be defined, and then, Equations 25 to 27 can be rewritten following Equation 28

$$\begin{cases} \hat{E}_y(\boldsymbol{\theta}) = \dfrac{1}{N}\displaystyle\sum_{k=1}^{N} g\left(x^{(k)}\right)\dfrac{f_X\left(\boldsymbol{x}^{(k)}\middle|\boldsymbol{\theta}\right)}{f_X\left(\boldsymbol{x}^{(k)}\middle|\boldsymbol{\theta}^*\right)} \\ \widehat{S^2}_y(\boldsymbol{\theta}) = \dfrac{1}{N}\displaystyle\sum_{k=1}^{N}\left(g\left(x^{(k)}\right) - E_y\right)^2 \dfrac{f_X\left(\boldsymbol{x}^{(k)}\middle|\boldsymbol{\theta}\right)}{f_X\left(\boldsymbol{x}^{(k)}\middle|\boldsymbol{\theta}^*\right)}, \\ \hat{P}_f(\boldsymbol{\theta}) = \dfrac{1}{N}\displaystyle\sum_{k=1}^{N} I_F\left(x^{(k)}\right)\dfrac{f_X\left(\boldsymbol{x}^{(k)}\middle|\boldsymbol{\theta}\right)}{f_X\left(\boldsymbol{x}^{(k)}\middle|\boldsymbol{\theta}^*\right)} \end{cases} \quad (20)$$

where I_F is the indicator function of failure expressed as $I_F(x) = 1$ if $x \in F$ (failure), and $I_F(x) = 0$ if $x \notin F$ (safety), $\hat{P}$ is the approximated failure probability, and $\widehat{S^2}_y$ is the approximation of the variance (second moment about the mean). For more details about cut-HDMR or complete equations for RS-HDMR, please refer to [17].

3.3 Confidence bounds and failure probability in dynamic problems using NISS and MCS

The application of NISS and MCS to static problems is straightforward. However, certain adjustments are required for dynamic problems. The proposed framework for calculating the confidence bounds involves the following steps:

1. Generate Time Signals: For each sample of the input variables, generate a time signal using deterministic simulation.
2. Group Solutions by Time Step: Organize the solutions from all time signals into groups corresponding to each time step, resulting in as many sets as there are time steps.
3. Process the data: Use each set of solutions as input for NISS (cut-HDMR or RS-HDMR) or the subsequent steps of Double-Loop MCS.

In the case of Double-Loop MCS, confidence bands (also called envelopes) can be constructed by determining the desired Probability Quantile (PQ) from the data collected at each time step. For the NISS-based approach, an additional hypothesis of normal distribution output is made. With that in mind, an optimization algorithm is needed to solve the following problems

$$Minimize\ f_{lb}(\boldsymbol{\theta}),$$
$$Subjected\ to\ \theta_{i\ min} \leq \theta_i \leq \theta_{i\ max}, i = 1, \dots, p, \tag{21}$$

$$Maximize\ f_{ub}(\boldsymbol{\theta}),$$
$$Subjected\ to\ \theta_{i\ min} \leq \theta_i \leq \theta_{i\ max}, i = 1, \dots, p, \tag{22}$$

here, p denotes the total number of epistemic parameters. For each epistemic parameter i, $\theta_{i\ min}$ and $\theta_{i\ max}$ represent the lower and upper limits, respectively. The functions $f_{lb}(\boldsymbol{\theta})$ and $f_{ub}(\boldsymbol{\theta})$ are defined as follows

$$f_{lb}(\boldsymbol{\theta}) = E_y(\boldsymbol{\theta}) - XS_y(\boldsymbol{\theta}), \tag{23}$$

$$f_{ub}(\boldsymbol{\theta}) = E_y(\boldsymbol{\theta}) + XS_y(\boldsymbol{\theta}). \tag{24}$$

In this context, E_y and S_y represent the output equations of the NISS method that approximate the mean and standard deviation, respectively, as detailed in Equations 17 to 20. These equations are computed in this study using the second-order cut-HDMR approach. For $X = 2$, the resulting bounds (envelopes) are expected to achieve approximately 95.45% confidence. The solutions to these minimization and maximization problems at each time step form the sets that constitute the final confidence bounds.

4 NUMERIC EXAMPLE: DISPLACEMENT CONFIDENCE BOUNDS

The dynamic structure simulated in this work consists of a Graphite AS4/Epoxy 3501-6 plate with a volume fraction of fibers $V_f = 0.6$. The laminate has a stacking sequence of $[30, -30, -30, 30]$ and is subjected to clamped-free-free-free boundary conditions.

The excitation force F is a sustained load applied at the tip of the plate described as normally distributed $F \sim \mathcal{N}(\mu_F, \sigma_F)$ with mean value of $\mu_F = F'[0.8, 1.2]\ N$ and standard deviation of $\sigma_F = F'[0.1, 0.2]\ N$, where $F' = -0.1\ N$. The longitudinal elastic modulus E_1 is also defined as normally distributed $E_1 \sim \mathcal{N}(\mu_{E_1}, \sigma_{E_1})$ with epistemic parameters mean $\mu_{E_1} = E_1'[0.8, 1.2]\ GPa$ and standard deviation $\sigma_{E_1} = E_1'[0.1, 0.2]\ GPa$. The value for E_1' is derived using the rule of mixtures and properties from Table 2, resulting in $E_1' = 138.2\ GPa$. Thus, the vector of epistemic parameters is defined as $\boldsymbol{\theta} = [\mu_{E_1}, \mu_F, \sigma_{E_1}, \sigma_F]$.

The quantity of interest, that is the vertical displacement z, along with a schematic representation of the composite plate is illustrated in Figure 2.

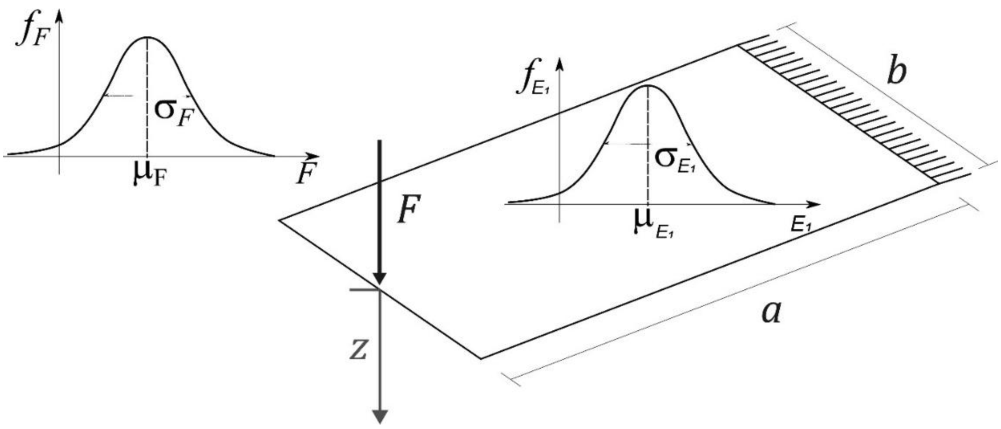

Figure 2: Composite plate diagram.

	$E\ [GPa]$	$\nu_{12}\ [-]$	$G_{12}\ [GPa]$	$\rho\ [kg/m^3]$
Fiber (Graphite AS4)	227.527	0.2	24.8211	1800
Matrix (Epoxy 3501-6)	4.2	0.340	1.567	1300

Table 2: Material Elastic properties extracted from MechG-Comp [25].

Newmark integration algorithm is applied to solve the finite element problem in time domain. The optimization algorithm used in the results presented in this work is the PSO [26] with the following parameters: number of particles, $n = 64$; momentum, $\omega = 0.95$; cognitive component 1 and 2, $C_1 = C_2 = 2.01$; tolerance, $tol = 10^{-6}$; maximum number of iterations, $nmax = 1{,}000$; random decay $\propto = 0.9$; and random perturbation, $\propto_t = 0.01$.

The final confidence bounds (envelopes) for the displacement can be seen in Figure 3, where the second order cut-HDMR was able to successfully capture the general behavior of the bound resulted by the Double Loop MCS. The total number of samples for the double-loop MCS was 800×800, while cut-HDMR was set to 2,000. Increasing the number of samples of NISS did not improve the solution, and the number of MCS samples was limited by the available computational resources.

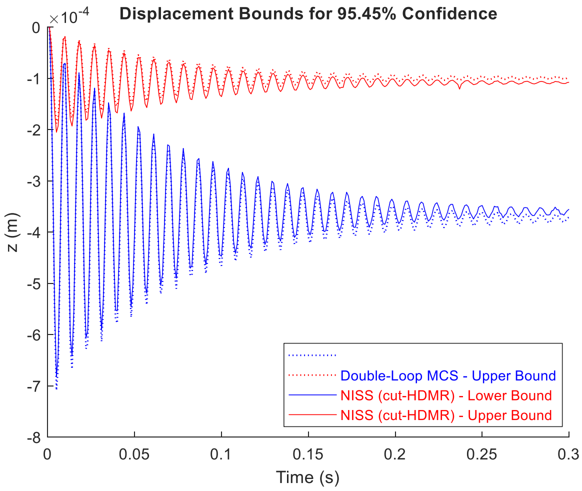

Figure 3: Displacement bounds for 95.45% confidence.

The RMS (root mean square) values of the time signals presented in Figure 3 can be checked in table 3, where the higher associated error found was 9.26% ($RMS_{Error} = (RMS_{\text{cut-HDMR}} - RMS_{MCS})/RMS_{MCS}$). This difference is attributed mainly to NISS precision and the normality hypothesis.

	RMS_{MCS} (m)	$RMS_{\text{cut-HDMR}}$ (m)	RMS_{Error} (%)
Upper Bound	0.1017×10^{-3}	0.1111×10^{-3}	9.26
Lower Bound	0.3838×10^{-3}	0.3695×10^{-3}	-3.72

Table 3: RMS values of the 95.45% confidence bounds found by Double-Loop Monte Carlo and NISS (second order cut-HDMR).

Figure 4 shows the design variables found by the optimization algorithm in each time step, revealing that some values of μ_{E_1} did not adhere to the maximum and minimum of the interval bound. While this behavior is atypical for static problems of the same nature, it can be attributed to the dynamic characteristics of the system. Variations in stiffness lead to shifts in the natural frequency of the system, resulting in intermediate values of μ_{E_1} as solutions to the optimization problem at specific time steps. Lastly, the confidence and behavior of each cut-HDMR in time domain for the mean $E(\boldsymbol{\theta})$ can be checked in Figure 5.

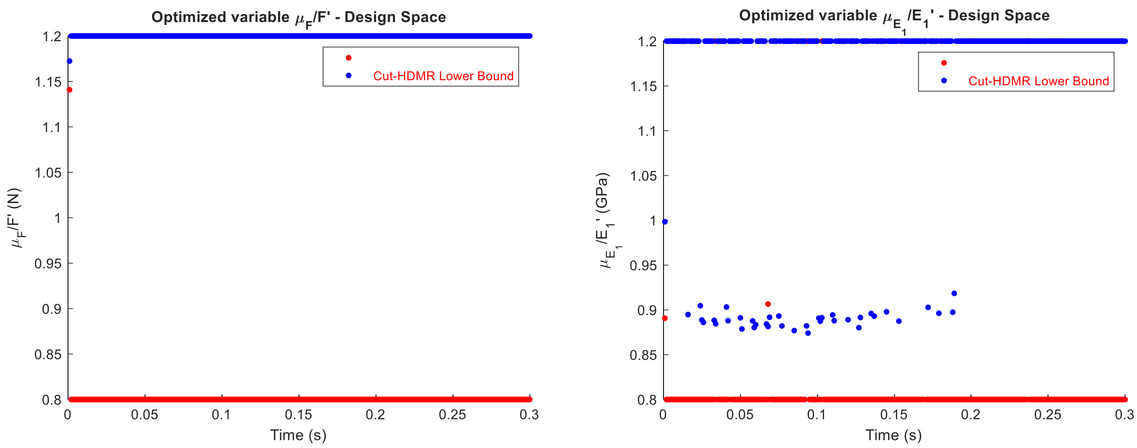

Figure 4: Optimized variables μ_{E_1} and μ_F in design space.

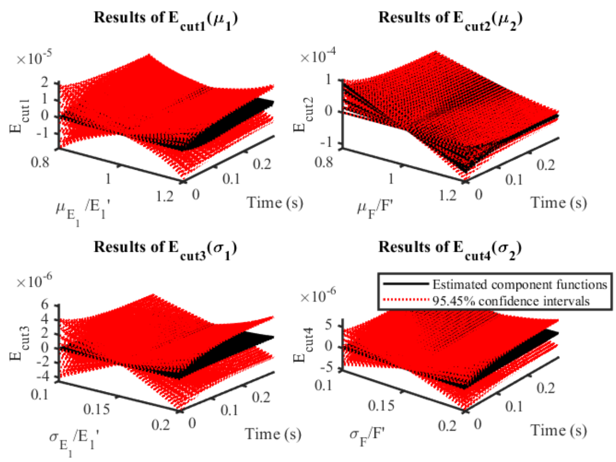

Figure 5: Confidence of each cut-HDMR component in time domain.

5 CONCLUSION

This study explores the confidence bounds and reliability problems in dynamic composite plates under epistemic uncertainties using NISS (cut-HDMR). The numerical example demonstrates the effectiveness of the presented framework employing cut-HDMR to estimate confidence bounds for vertical displacements in dynamic problems involving composite plates. Cut-HDMR successfully captures the overall behavior of the confidence bounds with great computational efficiency, requiring only 2,000 deterministic evaluations compared to 640,000 for double-loop MCS.

Future works may explore extending this framework to more complex structures and loading scenarios, incorporating advanced uncertainty modeling techniques. Additionally, further research could use the presented tools to investigate failure probability in composite plates.

FUNDING

This study is funded by CAPES/PROBRAL Project No.88887.895021/2023-00.

REFERENCES

[1] S. Dey, T. Mukhopadhyay, and S. Adhikari, *Uncertainty Quantification in Laminated Composites*. CRC Press, 2018.

[2] X. Li, Z. Lv, and Z. Qiu, A novel univariate method for mixed reliability evaluation of composite laminate with random and interval parameters, *Composite Structures*, vol. 203, pp. 153–163, Nov. 2018, doi: https://doi.org/10.1016/j.compstruct.2018.06.097.

[3] X.-Y. Zhou *et al.*, Bounds of mechanical properties of fibre reinforced polymer composites with hybrid random and interval uncertainties, *Thin-Walled Structures*, vol. 182, pp. 110158–110158, Oct. 2022, doi: https://doi.org/10.1016/j.tws.2022.110158.

[4] Matthias G.R. Faes, M. A. Valdebenito, D. Moens, and M. Beer, Operator norm theory as an efficient tool to propagate hybrid uncertainties and calculate imprecise probabilities, *Mechanical Systems and Signal Processing*, vol. 152, pp. 107482–107482, May 2021, doi: https://doi.org/10.1016/j.ymssp.2020.107482.

[5] D. Wu, A. Liu, Y. Huang, Y. Huang, Y. Pi, and W. Gao, Mathematical programming approach for uncertain linear elastic analysis of functionally graded porous structures with interval parameters, *Composites Part B Engineering*, vol. 152, pp. 282–291, Jun. 2018, doi: https://doi.org/10.1016/j.compositesb.2018.06.032.

[6] J. Zhu, Z. Lv, and H. Liu, A novel iterative algorithm for natural frequency analysis of FG thin plates under interval uncertainty, *Structural and Multidisciplinary Optimization*, vol. 60, no. 4, pp. 1389–1405, May 2019, doi: https://doi.org/10.1007/s00158-019-02267-x.

[7] L. Wang, Y. Liu, and Y. Liu, An inverse method for distributed dynamic load identification of structures with interval uncertainties, *Advances in Engineering Software*, vol. 131, pp. 77–89, May 2019, doi: https://doi.org/10.1016/j.advengsoft.2019.02.003.

[8] C. Xiong, L. Wang, G. Liu, and Q. Shi, An iterative dimension-by-dimension method for structural interval response prediction with multidimensional uncertain variables, *Aerospace Science and Technology*, vol. 86, pp. 572–581, Mar. 2019, doi: https://doi.org/10.1016/j.ast.2019.01.032.

[9] S. Dey, T. Mukhopadhyay, H. H. Khodaparast, and S. Adhikari, Fuzzy uncertainty propagation in composites using Gram–Schmidt polynomial chaos expansion, *Applied Mathematical Modelling*, vol. 40, no. 7–8, pp. 4412–4428, Apr. 2016, doi: https://doi.org/10.1016/j.apm.2015.11.038.

[10] M. D. F. Awruch and H. M. Gomes, A fuzzy α-cut optimization analysis for vibration control of laminated composite smart structures under uncertainties, *Applied Mathematical*

Modelling, vol. 54, pp. 551–566, Feb. 2018, doi: https://doi.org/10.1016/j.apm.2017.10.002.

[11] H. Lü, Wen-Bin Shangguan, and D. Yu, Uncertainty quantification of squeal instability under two fuzzy-interval cases, *Fuzzy Sets and Systems*, vol. 328, pp. 70–82, Jul. 2017, doi: https://doi.org/10.1016/j.fss.2017.07.006.

[12] H. Lü, Z. Cai, Q. Feng, Wen-Bin Shangguan, and D. Yu, An improved method for fuzzy–interval uncertainty analysis and its application in brake instability study, *Computer Methods in Applied Mechanics and Engineering*, vol. 342, pp. 142–160, Dec. 2018, doi: https://doi.org/10.1016/j.cma.2018.07.028.

[13] P. B. Santana, Ewerton Grotti, and H. M. Gomes, An Efficient Anti-Optimization Approach for Uncertainty Analysis in Composite Laminates, *Materials Research*, vol. 24, no. suppl 2, Jan. 2021, doi: https://doi.org/10.1590/1980-5373-mr-2021-0334.

[14] K. Zhou, Z. Wang, Q. Gao, S. Yuan, and J. Tang, Recent advances in uncertainty quantification in structural response characterization and system identification, *Probabilistic Engineering Mechanics*, vol. 74, pp. 103507–103507, Aug. 2023, doi: https://doi.org/10.1016/j.probengmech.2023.103507.

[15] R. Schöbi and B. Sudret, Global sensitivity analysis in the context of imprecise probabilities (p-boxes) using sparse polynomial chaos expansions, *Reliability Engineering & System Safety*, vol. 187, pp. 129–141, Jul. 2019, doi: https://doi.org/10.1016/j.ress.2018.11.021.

[16] H. Xie, J. Li, and D. Liao, A new structural reliability analysis method under non-parameterized probability box variables, *Structural and Multidisciplinary Optimization*, vol. 65, no. 11, Nov. 2022, doi: https://doi.org/10.1007/s00158-022-03408-5.

[17] P. Wei *et al.*, Non-intrusive stochastic analysis with parameterized imprecise probability models: I. Performance estimation, *Mechanical Systems and Signal Processing*, vol. 124, pp. 349–368, Jun. 2019, doi: https://doi.org/10.1016/j.ymssp.2019.01.058.

[18] P. Wei *et al.*, Non-intrusive stochastic analysis with parameterized imprecise probability models: II. Reliability and rare events analysis, vol. 126, pp. 227–247, Jul. 2019, doi: https://doi.org/10.1016/j.ymssp.2019.02.015.

[19] J. Song *et al.*, Generalization of non-intrusive imprecise stochastic simulation for mixed uncertain variables, *Mechanical Systems and Signal Processing*, vol. 134, pp. 106316–106316, Dec. 2019, doi: https://doi.org/10.1016/j.ymssp.2019.106316.

[20] J. Song, M. Valdebenito, P. Wei, M. Beer, and Z. Lu, Non-intrusive imprecise stochastic simulation by line sampling, *Structural Safety*, vol. 84, pp. 101936–101936, Feb. 2020, doi: https://doi.org/10.1016/j.strusafe.2020.101936.

[21] H. Zhao and C. Zhou, An imprecise multiscale uncertainty quantification framework for fiber reinforced composites, *Probabilistic Engineering Mechanics*, vol. 78, pp. 103686–103686, Sep. 2024, doi: https://doi.org/10.1016/j.probengmech.2024.103686.

[22] O.C. Zienkiewicz, R.C. Taylor, *The finite element method, Vol. I, 4th Edition*. McGraw Hill, 1989.

[23] A J M Ferreira and G M L Gladwell, *MATLAB Codes for Finite Element Analysis : Solids and Structures*. Dordrecht: Springer Netherlands, 2009.

[24] A. K. Kaw, *Mechanics of Composite Materials*. Boca Raton Crc Press, 2005.

[25] Grupo de Materiais Compósitos e Nano Compósitos, 2025. Mech G-comp, www.ufrgs.br/mechg.

[26] J. Kennedy and R. Eberhart, Particle swarm optimization, *Proceedings of ICNN'95 - International Conference on Neural Networks*, vol. 4, pp. 1942–1948, 1995, doi: https://doi.org/10.1109/icnn.1995.488968.